Tribology International 209 (2025) 110716

Contents lists available at ScienceDirect

Tribology International

journal homepage: www.elsevier.com/locate/triboint

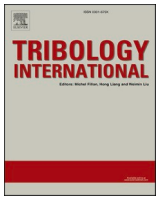

Nitrogen alloyed $MoSe_2$ coatings – Role of optimized morphology, structure and mechanical properties on diverse environment sliding performance

Talha Bin Yaqub [a,b,*], Irfan Nadeem [b], Filipe Fernandes [a,d], Khurram Yaqoob [e], Mitjan Kalin [b], Albano Cavaleiro [a,c]

[a] University of Coimbra, CEMMPRE, ARISE, Department of Mechanical Engineering, Rua Luís Reis Santos, Coimbra 3030-788, Portugal
[b] Laboratory for Tribology and Interface Nanotechnology, University of Ljubljana, Bogišićeva 8, Ljubljana 1000, Slovenia
[c] IPN - LED&MAT - Instituto Pedro Nunes, Laboratório de Ensaios, Desgaste e Materiais, Rua Pedro Nunes, Coimbra 3030-199, Portugal
[d] CIDEM, ISEP, Polytechnic of Porto, Rua Dr. António Bernardino de Almeida, 431, Porto 4249-015, Portugal
[e] School of Chemical and Materials Engineering (SCME), National University of Sciences and Technology (NUST), H-12, Islamabad, Pakistan

ARTICLE INFO

Keywords:
Friction and wear
MoSeN coatings
TMDs
PVD sputtering
Diverse environment sliding

ABSTRACT

Transition metal dichalcogenide (TMD) coatings are gaining increasing interest among the scientific community as eco-friendly solutions for reducing friction, improving energy conservation, and lowering carbon footprints. N-alloyed $MoSe_2$ coatings (MoSeN), a subset of TMDs, remain largely underexplored, with no research on their frictional performance across various sliding environments. Herein, an in-depth analysis of DC-magnetron sputtered MoSeN coatings is presented, with N content varying from 0 to 42 at%. Investigation of composition, morphological features, crystal structure, mechanical strength and sliding performance are accessed. Our findings revealed that N additions resulted in increased compactness, amorphous structure and hardness of ~4.6 GPa, and these improvements remained consistent despite compositional variations. The sliding competency was evaluated under six different conditions, revealing promising results in ambient-air and dry-N_2 atmospheres at room conditions and 100 °C. At 200 °C, the sliding performance in ambient-air was better than dry-N_2. Friction coefficient for N-alloyed coatings was relatively close, ranging between 0.03 and 0.06, except for a dry-N_2 environment at 200 °C. Nevertheless, wear rate showed slight variations, with higher values observed in dry-N_2 at 100 °C and 200 °C but remained within a specific range of 1–7 × 10^{-7} mm^3/Nm for all other conditions. This study highlights the potential of MoSeN coatings to be scaled for industrial applications, offering a roadmap for reducing the inherent limitations of PVD sputtering.

1. Introduction

The current global landscape is rapidly evolving towards industry 5.0, driven by technological innovations in processes and systems [1]. This transition necessitates the implementation of highly efficient, cost-effective, and state-of-the-art manufacturing and operational processes. An important aspect of this evolution is the emphasis on environmentally friendly solutions that align with the Sustainable Development Goals of United Nations and European Union and this shift has become quite swift nowadays due to the advent of the latest technologies in processes and systems. The same cannot be achieved without the use of highly efficient, low cost and state of the art manufacturing as well as operational processes. This urge coupled with green manufacturing in line with UN and EU sustainable development goals [2,3]. Consequently, the modern research institutions and industrial sectors are prioritizing sustainable practices [4]. Environmental protection regulations now stipulate that both processes and products must comply with green initiatives. Achieving these demands requires creating an environment that supports energy conservation while being self-sustaining [3,5].

Given the focus on these needs, the automotive and aerospace industries are continually adapting practices that balance economic efficiency, environmental sustainability, and extended life cycles. A considerable development in this context is the shift towards electric vehicles (EVs) and the use of materials that reduce or eliminate the need for liquid lubricants, while maintaining or enhancing economic efficiency [6]. Although liquid lubricants have been widely used for a long time, they have inherent issues that are becoming increasingly

* Corresponding author at: Laboratory for Tribology and Interface Nanotechnology, University of Ljubljana, Bogišićeva 8, Ljubljana 1000, Slovenia.
E-mail address: talhabin.yaqub@fs.uni-lj.si (T.B. Yaqub).

https://doi.org/10.1016/j.triboint.2025.110716
Received 21 October 2024; Received in revised form 3 April 2025; Accepted 7 April 2025
Available online 8 April 2025

problematic in the modern world [7–9]. Key issues highlighted by environmental protection agencies and industry include vitalization and degradation, economic losses due to degradation and leakage, harmful emissions that are detrimental to both the environment and human health, corrosion and oxidation damage, and inefficiency in diverse environments sliding such as aerospace mobility applications [10–13].

Considering the adverse effects and inherent drawbacks of conventional lubricants, researchers in the field of green tribology and green mobility have introduced solid lubricant coatings as an alternative for aerospace, EVs, and related applications in which long-term lubrication, weight reduction, energy conservation, and sustainability are paramount concerns [6,14]. Furthermore, solid lubricants not only combat the concerning issues of liquid lubricants, but also support the production of higher quality products, lean manufacturing processes, enhanced production efficiency, and cost reduction[15]. Consequently, these lubricants are gaining sufficient popularity in current times due to their excellent sliding characteristics [16–19]. Different solid lubricious materials have been researched in past few decades, including DLCs[20], WC with C [21], Mo and W doped films [22,23], various types of TMD coatings [18,24–27], and metallic materials which are ductile and shear easily [19,28,29].

TMDs have recently gained prominence among researchers and industries involved in aerospace mobility, primarily due to their low friction properties in vacuum environments [15]. These properties stem from their unique lamellar structure, with a high degree of anisotropy [30–34]. The TMD compounds are represented by X-M-X formula (M=metal atom, X = chalcogen atom) where, 6 chalcogens surround each metal atom. This configuration features strong covalent bonding within the chalcogen-metal-chalcogen layer and a weak van-der Waals bond exists between these layers, facilitating easy sliding and resulting in a low friction [35,36]. However, sputtered TMDs have a porous morphology, resulting in low load-bearing capabilities, low hardness, weak adhesion to substrates, and high moisture sensitivity due to increased surface area, restricting their excessive utilization for sliding under diverse environments [25,37–40]. Fortunately, in the late 90 s, Voevodin's work proved to be a ray of hope when he combined TMDs with amorphous carbon and showed that the tribological properties of TMDs could be significantly enhanced, making them suitable for multi-environment sliding applications [32]. Since then, intensive research into the development of TMD-based coatings has led to promising output.

The present authors have devoted considerable effort to optimizing TMD-based solid lubricants alloyed with carbon (C) and nitrogen (N). Various successful approaches have been reported in recent years, including TMD-alloying with non-metals (C and N) [30,31,37,41–45]. Among these, the primary focus has been on optimizing C-alloyed TMDs, which exhibit low friction properties across diverse environments. Here, a multi-target sputtering approach was used, which is comparatively less cost-effective than reactive sputtering [44]. Reactive sputtering with C alloying was avoided due to the potential contamination of the coatings by precursor gases such as CH_4 and C_2H_2 [46,47]. Therefore, the reactive sputtering with N becomes the only option. Using N gas offers several advantages: (i) it can be used in its pure N_2 form, (ii) results in compact coatings similar to those achieved with C alloying, and (iii) allows the N-alloyed atoms to escape the wear track as N_2, which ultimately favours the formation of a pure TMD-based tribolayer [48–51]. N-alloyed WS_2 and MoS_2 have already been studied in detail, whereas the N-alloying of $MoSe_2$ has remained less explored. TMD coatings made from $MoSe_2$ offer excellent sliding properties in dry, vacuum, and ambient conditions compared to other TMD coatings [52,53].

Therefore, considering the advantages of N alloying with TMDs, the maiden attempt to develop N-alloyed $MoSe_2$ coatings (MoSeN) using DC sputtering was reported by the current authors [43]. Prior to this, only one study focused on these coatings deposited via HiTUS method was reported [54]. In comparison to the latter study, the findings reported by the present authors revealed unique properties of MoSeN coatings, marking a significant advancement in overcoming the inherent drawbacks of PVD sputtering. Typically, PVD is a line-of-sight sputter deposition process and thus, achieving uniform/homogeneous coatings on complex surfaces, leading to inconsistencies in composition. Such variations can lead to non-uniform coatings, which increases performance degradation leading to the risk of potential failures, and often hampers the industrial application of these coatings [55]. Addressing these concerns, the DC-sputtered MoSeN coatings with varying compositions were tested, and it was found that their tribological properties remained consistent [43]. This demonstrates that the compositional differences did not significantly impact the performance of the DC sputtered MoSeN coatings.

It is important to highlight that prior work focused exclusively on testing in ambient air (AA) at room temperature conditions (RT). Therefore, further investigation of MoSeN system is required to evaluate the efficiency of the tribological properties with varied compositions when subjected to sliding in diverse environments. Such analysis is essential for unlocking the full potential of these coatings in applications involving diverse environmental conditions. If successful and efficient performance is achieved, these coatings could be considered ideal for use in complex 3D components, such as in EVs and the aerospace industry, where sliding in varied environments is common. It is well established in literature that TMDs alloying with different elements were developed to enhance the fundamental and diverse environment sliding properties of these coatings. However, conventionally, the literature only deals with room temperature ambient air, high temperature (100 °C and 200 °C) and dry atmosphere sliding. This dry atmosphere can be vacuum or a replication of non-humid conditions like sliding in dry-N_2. Thus, dry-N_2 is used to remove the moisture from the sliding atmosphere. Moreover, the literature studies rarely study high temperature sliding in dry-N_2 atmosphere which has been accessed in this work. Considering this need in mind, the present research is designed to address the diverse environment sliding characteristics by investigating the sliding properties of optimized MoSeN coatings. Thus, this study explores their performance in both AA and dry-N_2 environments over a range of temperatures, including room and elevated temperatures.

2. Experimental details

2.1. Coating synthesis

For this process, only two cathodes, i.e., $MoSe_2$ and Cr, were used during the deposition. Prior to MoSeN deposition, the Cr-target was utilised for adhesion and gradient under layers. The purity and dimensions of these targets were 99.9 %, and (380 x 175 x 8) mm, respectively. All coatings were deposited in Ar gas atmosphere with a steady flow rate of 35 sccm, while N with varying flow rates from 0 to 10 sccm was used for depositing a set of reactively sputtered MoSeN coatings. The chamber pressure was maintained at 0.27 Pa throughout the deposition process by carefully balancing the flows of N and Ar gases. The schematic of the deposition chamber and arrangement of targets is shown in Fig. 1.

Polished silicon (Si) wafer substrates were coated to evaluate various coating properties such as chemical composition, surface and cross-sectional morphology, deposition rate, crystal structure, and mechanical properties. For tribological testing, AISI 52100 steel (Ø25 mm x 7 mm) was used as substrate. Prior to coating deposition, steel substrates were mirror polished using rough grinding and diamond polishing. This was followed by ultrasonic cleaning of the substrate in acetone and ethanol to ensure surface cleanliness. Later, they were glued to substrate holder placed 15 cm away from the targets. The base pressure and substrate rotation were fixed to $\sim 7 \times 10^{-4}$ Pa and 10 rev/min, respectively.

The deposition process began with a thorough etch cleaning of both the targets and substrates. Substrates etch-cleaning was performed for 40 minutes by a 600 V pulsed-DC voltage and 250 kHz frequency. In

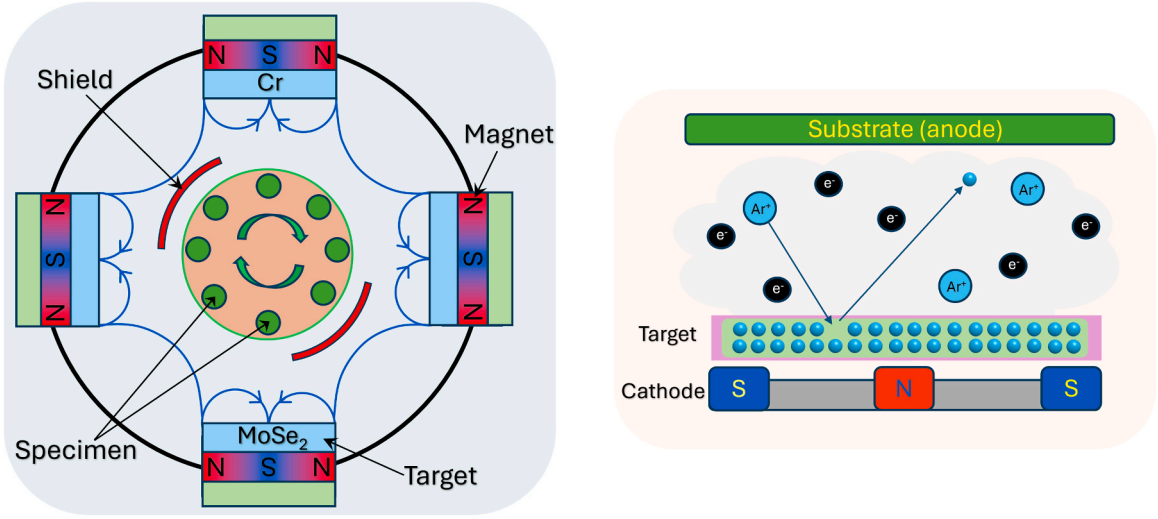

Fig. 1. Schematic of sputtering system and interactions occurring in the vicinity of target electrode.

parallel, the Cr and $MoSe_2$ targets were sputtered for 20 minutes each, using currents of 3.0 A and 1.4 A, respectively. Shutters were employed in front of targets to avoid cross-contamination during this phase. The second phase involved the deposition of a Cr-interlayer in current control mode, using a current of 5.0 A for 15 minutes and under 600 V substrate bias. Next, a gradient layer was deposited over a period of 5 minutes, whereby the current on the $MoSe_2$ target was linearly increased to 1.51 A and the current on the Cr target was reduced to zero. Finally, the last phase was to deposit the outer/final coating with 50 V substrate bias at 250 kHz frequency. Here, the current on the $MoSe_2$ target was kept constant at 1.4 A. To achieve variable composition of the MoSeN coatings, the N_2 gas flow rate was varied from 0 to 10 sccm. The deposition time was adjusted to produce coatings with a thickness of approximately 2 μm. Table 1 provides details of the set of deposited coatings and the key deposition parameters.

2.2. Characterization of coatings

The cross-sectional and surface morphologies were examined using field-emission scanning electron microscopy, FESEM (Zeiss Merlin, Germany). The surface morphologies were analysed directly, while the cross-sectional morphologies were examined on freshly cut samples to accurately measure the coating thickness. To measure chemical composition, wavelength dispersive spectroscopy, WDS (Oxford Instruments, United Kingdom) was employed operating under 15 kV accelerating voltage. Calibration of WDS instrument was performed prior to the measurements, using certified standards provided by Micro Analysis Consultants to ensure the accuracy and reliability of the results.

The crystal structure analysis was done in X-ray diffractometer (PANalytical, Netherlands) particularly to determine the presence of $MoSe_2$ and MoN phases. The analysis was performed using Cu $K_{\alpha 1}$, $\lambda = 1.5406$ Å source, with the system set to operate in grazing incidence mode at an angle of 3°.

The mechanical properties were retrieved using nanoindentation (Micro Materials Nanotest platform). A Berkovich diamond indenter with an applied load of 3 mN was used. To ensure accuracy, two sets of 16 indentations each were made on each sample, and the mean value was calculated. 3 mN load was carefully chosen so that the depth of indentation remains below 10 % of the total thickness of coating. The measured reduced elastic modulus and hardness values were further used to determine the H/E* and the H^3 /E* of the MoSeN coatings.

Sliding performance efficiency studies were conducted against a 10 mm 100Cr6 ball as counter body, under controlled conditions of 25 °C in AA (25 – 35 % relative humidity) as well as in a dry-N_2 atmosphere. Additional testing was also conducted at elevated temperatures of 100 °C and 200 °C in both these environments, simulating a wide range of operating conditions to examine sliding performance in diverse environments. All tests were carried out using an SRV tribometer operating in a reciprocating sliding motion (Optimol Instruments, Germany). Test parameters included 10 N load (corresponding to an initial Hertzian contact stress of ~1 GPa), 25 Hz sliding frequency, 2 mm stroke length, 0.1 m/s sliding velocity, and 1200 seconds test duration. These conditions were selected in accordance with most of the literature on C and N alloyed WS_2, MoS_2 and $MoSe_2$ coatings [27]. The conditions were also similar to the ones reported in our previous work [43]. This consistency with literature and our previous work has been maintained to enable a better comparison of different systems and their performance. Prior to testing, 10 minutes ultrasonic cleaning of sliding pairs was done in acetone and ethanol, each to ensure cleanliness and remove any surface contaminants.

The wear tracks of coatings were examined under a digital light microscope (Hirox HRX-01, Japan). To quantify the specific wear rate (*WR*), wear profiles were measured at 3 points along the track using stylus profilometer (Surftest SJ-500, Japan). After the sliding tests, Raman mapping was performed within the track of selected coating to investigate tribo-induced structural changes and to assess the surface coverage. Measurements were carried out from 100 to 600 cm^{-1} wavenumber under 532 nm laser (XploRA, Horiba). Particular attention was given to the selection of the appropriate acquisition settings to prevent any damage to the surface during the analysis.

Additionally, a selected MoSeN coating was also exposed to high temperature of 400 °C to examine the influence of temperature and oxidation in high temperature sliding testing. This temperature was chosen to accelerate the impact of thermal exposure beyond testing condition of 200 °C. For this analysis, the 400 °C exposed coating was analysed in SEM. Moreover, for the same investigation purposes, a similar coating was also exposed to in-situ XRD at 25 °C and 400 °C.

Table 1
Key deposition parameters for the coatings deposition.

Coatings	$MoSe_2$ target current (A)	Nitrogen flow rate (sccm)	Substrate bias (V)	Substrate to target distance (cm)
C1	1.4	0	50	15
C2		1.7		
C3		5		
C4		10		

3. Analysis results

3.1. Morphology, composition and structure

The morphological results of the $MoSe_2$ and MoSeN coatings are presented in Fig. 2a and b. One set of representative micrograph is shown for the N containing coatings (Fig. 2b) to illustrate the typical morphology of all MoSeN coatings. The C1 (pure $MoSe_2$) coating without N-alloying (0 at% N) exhibited a columnar and porous cross-section and surface morphologies (Fig. 2a). In contrast, after nitrogen alloying, the surface morphology transformed into a highly compact, cauliflower-like feature (Fig. 2b). The cross-sectional images similarly revealed the elimination of the columnar features, which were replaced by densely packed morphology, reflecting the increase in compactness of the N-alloyed coatings (see inset of Fig. 2b).

The composition of all deposited coatings, including the N content and its effect on Se/Mo ratio, as measured by WDS, is shown in Fig. 2c. The C1 coating ($MoSe_2$), with 0 at% N content exhibited Se/Mo = 2, which means that the coating is stoichiometric. This is notable, as the achieved stoichiometry for C1 coating is higher than what is typically observed for other sputtered TMDs such as MoS_2 and WS_2, which may contribute to improved tribofilm formation and enhanced sliding properties [26,55–57]. With the addition of nitrogen in the deposition unit, the N in the coatings gradually increased, causing the chemical composition to deviate from the ideal stoichiometry. The C2 coating, deposited with a nitrogen flow of 1.7 sccm, showed an N content of about 21 at% and a corresponding reduction in the Se/Mo ratio to 1.8. With further increase in nitrogen flow to 5 and 10 sccm, the N content increased to 35 at% and 42 at%, respectively, while the Se/Mo ratio decreased to 1.6 and 1.4, respectively. This gradual shift reflects the significant influence of the N-alloying on the coating's composition. The deposition rate of the C1 coating initially measured around 16 nm/min but decreased to approximately 12 nm/min with the addition of 22 at% nitrogen. As the nitrogen content was further increased to 35 at%, the deposition rate dropped again to about 10 nm/min. Finally, with 42 at% nitrogen, the coating exhibited the lowest deposition rate of approximately 7 nm/min. This decreasing trend can be attributed to the increased compactness of the coating, a reduced Se/Mo ratio, and the inherently slower deposition rates typical of ceramic materials.

The structural analysis of the coatings, performed in grazing incidence mode (3°), is shown in Fig. 2d. The C1 coating, representing pure $MoSe_2$ (0 at% N), exhibited an XRD pattern characteristic of typical sputtered TMDs, with well-defined peaks corresponding to the $MoSe_2$ crystal structure (ICCD No. 087–2419). Since the analysis was performed in grazing incidence mode, the prominent peak observed at ~13° corresponds to the (002) basal planes, inclined at about 5° from the surface, indicating that these planes are nearly parallel to the coating surface. Additionally, the peaks pertaining to (10 L) planes (here, L = 1, 2, 3, …) with extended shoulders towards higher angles, detected in the ~30–50° range, are indicative of turbostratic stacking, as described by Weise et al. [56]. With N incorporation, the crystal structure became amorphous, causing the disappearance of the (002) peak. However, a broad peak was detected in the ~30 – 50° range. Similar amorphous behaviour was observed with increasing nitrogen content. Therefore, only one representative XRD pattern is shown for all MoSeN coatings. Additional peaks from the Cr interlayer were also identified and are marked in Fig. 2d.

3.2. Mechanical characteristics

The mechanical characteristics of all coatings, including the hardness, the (reduced) modulus of elasticity, the fracture toughness and the

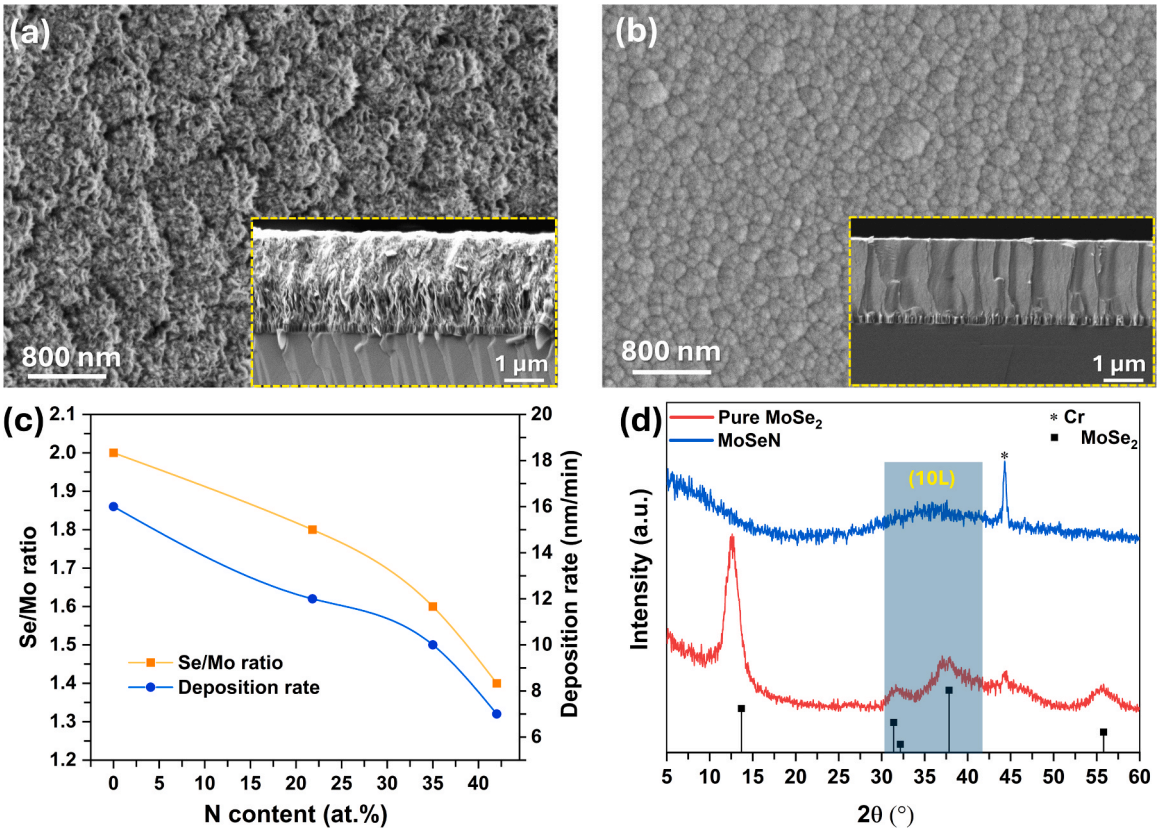

Fig. 2. (a) Surface and cross-sectional morphologies of Pure $MoSe_2$ coating, (b) Surface and cross-sectional morphologies of one MoSeN coating as representative of all N-alloyed coatings, (c) Impact of N content variations on Se/Mo ratios and deposition rates of deposited coatings, and (d) Crystal structure of Pure $MoSe_2$ coating and one MoSeN coating as representative of all N-alloyed coatings.

elastic strain to failure, analysed using the nanoindentation technique, are presented in Fig. 3. The observed trends align closely with the compositional, morphological, and structural characteristics of the coatings shown earlier. The coating without N-alloying exhibited a hardness value of 1 GPa, while all MoSeN coatings showed significantly higher hardness values in the range of about 4.4 – 4.6 GPa (Fig. 3a). Based on our previous studies with TMD-based coatings [45], these hardness values are sufficient for providing good load sustainability and in turn promising sliding properties.

In line with the trends in hardness, the reduced elastic modulus also increased with the addition of N (Fig. 3a). Likewise, the elastic strain to failure [58] and fracture toughness [59] parameters, which are shown in Fig. 3b, were also significantly increased by the N-alloying.

3.3. Tribological performance

To thoroughly and comprehensively analyse the sliding properties of MoSeN coatings with the aim of industrial penetration, the testing was performed under six distinct conditions. This section presents the friction coefficient (COF) and specific wear rate (*WR*) results obtained from these varied tests, offering valuable insights into the performance and durability of the coatings.

3.3.1. Sliding in ambient air atmosphere at room temperature

The average COF for all coatings tested in AA at RT is shown in Fig. 4a. This average value was calculated during the steady-state region of sliding. The C1 coating exhibited the highest value of COF i.e., ~0.075. However, N-addition in coatings helped the COF to decrease, with the average COF value for the C2 coatings dropping to around ~0.055. Interestingly, further increases in N-alloying did not lead to any significant changes in COF, which remained stable at around 0.055 – 0.06. This indicates that the coatings exhibited consistent frictional properties in this condition despite variations in composition.

Fig. 4b presents the *WR* results obtained after sliding in this environment. The C1 coating had the lowest *WR* among all the samples, measuring 3.5 x 10^{-7} mm^3/Nm. However, with the introduction of N, the *WR* increased slightly to 4×10^{-7} mm^3/Nm. Like the trends observed for COF, the *WR* of the MoSeN system in this environment remained consistent, regardless of the N content, and were close to 4×10^{-7} mm^3/Nm, implying negligible impact on wear performance with increased N-alloying.

The wear track images obtained from the tribological tests are shown in Fig. 4c. The C1 coating appears to be well-covered by a tribolayer, which is consistent with the observed sliding results (Fig. 4c-i). In contrast, the N-alloyed coatings show signs of abrasive wear, probably hard wear particles generated due to sliding. In addition, the width of worn tracks is greater for the N-alloyed coatings than for the C1 coating, despite coverage of the tracks by the TMD tribolayer displayed minor differences (see Fig. 4c (i-iv)). This observation further supports the marginal increment in *WR* for the MoSeN coatings.

3.3.2. Sliding in ambient air atmosphere at 100 °C

The steady-state average COF for the coatings after sliding in AA atmosphere at 100 °C are presented in Fig. 5. As shown in Fig. 5a, the C1 coating exhibited a COF of ~0.09, which is higher than the values observed at room temperature. In contrast, the C2 coating maintained a COF of ~0.06, which is almost identical to the results at room temperature. Further increasing the N content led to a COF value of ~0.045 for the C3 coating, which is slightly lower than the measurement at room temperature. For C4 having maximum N, a COF value of ~0.058 was recorded. Overall, the COF values remained relatively consistent across the different coatings with negligible difference. Within this negligible difference, C3 exhibited the lowest COF, with a difference of only 0.01 compared to the other MoSeN coatings.

The *WR* for the C1 coating was maximum i.e., 6.4 x 10^{-7} mm^3/Nm (Fig. 5b). However, with the introduction of N, the *WR* for the C2 coating decreased significantly to 1.5×10^{-7} mm^3/Nm. The *WR* of 2×10^{-7} mm^3/Nm was measured for C3 coating, which was lower than for the C1 coating, but still higher than for the C2 coating. Lastly, the C4 coating exhibited *WR* of 2.3×10^{-7} mm^3/Nm. Overall, the *WR* decreased compared to RT results. These decrements are quite minorly better than the room temperature tests.

Fig. 5c shows the worn track optical images of the C1 and MoSeN coatings. The track of the C1 coating is mainly covered by a $MoSe_2$ tribolayer; however, the underlying layers are slightly exposed, with the thickness of the wear track being greater than that of the N-alloyed coatings. This exposure of the underlayers contributes to the high *WR* of the C1 coating (see Fig. 5c-i). In contrast, the MoSeN coatings exhibited excellent coverage of their wear tracks, which effectively supported sliding with a low COF. No evidence of underlayer exposure was observed in these coatings, reinforcing the observed decrease in *WR* values.

3.3.3. Sliding in ambient air atmosphere at 200 °C

After preliminary testing at 200 °C, it was observed that the coatings could not sustain the initially selected duration of 1200 seconds. Therefore, the test duration was shortened to 600 seconds to avoid entering a state of complete failure or gross delamination of the coatings. Thus, the increase in temperature to 200 °C resulted in significant changes in performance compared to the previously reported conditions (Fig. 6a). Notably, the C1 coating exhibited the lowest COF of ~0.042, a value that is the least in all testing conditions for the C1 coating. Throughout most of the test, the COF fluctuated between ~0.025 and ~0.05. C2 and C3 coatings had almost identical results of ~0.032 and

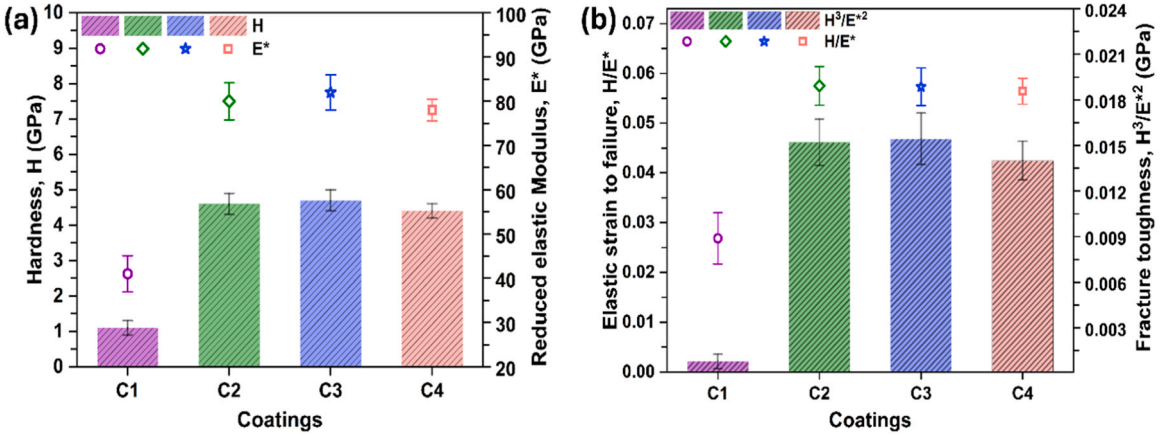

Fig. 3. (a) Hardness (H) and reduced elastic modulus (E*), and (b) Elastic strain to failure ratio (H/E*) and fracture toughness (H^3/E^{*2}) of the deposited coatings.

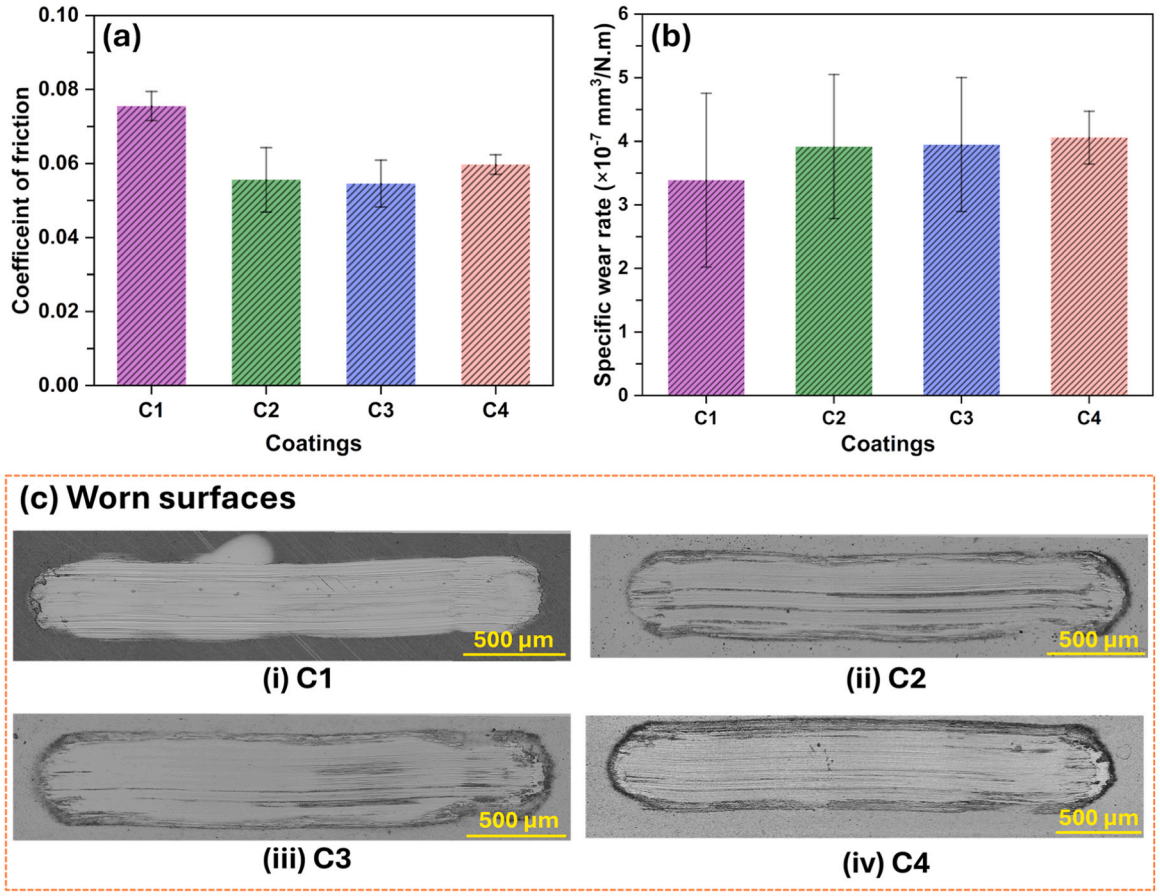

Fig. 4. (a) Friction coefficients, (b) Specific wear rates, and (c) Optical images of worn tracks of MoSeN coatings in ambient air at room temperature.

~0.03, respectively. However, with a further increase of N, the COF value increased to ~0.038 for the C4 coating. These COF values were the lowest observed under ambient air atmosphere conditions.

The C1 coating exhibited a W*R* of 6×10^{-7} mm^3/Nm, which is twice as high as at room temperature and equivalent to the value at 100 °C (Fig. 6b). In contrast to the trends observed for the COF, the W*R* for the N-alloyed coatings increased in comparison to 100 °C testing results. The C2 coating had a W*R* of 3×10^{-7} mm^3/Nm, while the C3 coating displayed 4×10^{-7} mm^3/Nm W*R*. Both of these values were comparable to those from room temperature testing but higher than the results at 100 °C. The C4 coating with maximum N, displayed the highest W*R* i.e., 7×10^{-7} mm^3 /Nm, which was the highest among all the tests conducted in an ambient air atmosphere.

The wear tracks for the C1 and MoSeN coatings are presented in Fig. 6c. The C1 coating exhibited wear tracks characterized by the presence of a tribolayer, which contributed to the reduction in friction, along with areas of underlayer exposure. Notably, this exposure increased as the testing conditions transitioned from 100 °C to 200 °C. In the case of the MoSeN coatings (Fig. 6c (ii-iv)), the wear tracks were predominantly covered by tribo-layer zones in the central areas. However, delamination was observed at the edges and at a few locations along the centreline of the track, indicating localized failures despite the coverage. It should also be noted that the delamination at edges increased with increasing N content.

3.3.4. Sliding in dry-N_2 atmosphere at room temperature

To access the sliding efficiency of coatings in non-humid dry conditions, testing was conducted in a dry-N_2 atmosphere. In the first analysis, the coatings were allowed to slide at room temperature in dry-N_2 filled chamber (results shown in Fig. 7a). The C1 coating exhibited an average COF of ~0.07, which decreased to ~0.03 as the N content in coating increased (i.e., C2 coating). The C3 coating achieved a COF of ~0.025, which was the lowest value recorded in this condition, as well as under all testing conditions. However, with a further increase in N content, the COF increased to ~0.039 for the C4 coating. Overall, the COF remained very stable throughout the tests in this environment, and the results were among the lowest for MoSeN coatings across all tested conditions.

The W*R* results are presented in Fig. 7b. The C1 coating showed a low W*R* 2×10^{-7} mm^3/Nm, which increased to 5×10^{-7} mm^3/Nm for C2 coating. Interestingly, the W*R* decreased to 2×10^{-7} mm^3/Nm for the C3 coating. The coating with maximum N, i.e., C4, displayed the lowest W*R* of 1×10^{-7} mm^3/Nm. Overall, the W*R* achieved for the C3 and C4 coatings were the lowest, while, for the C2 coating, the value was highest in this test condition.

The worn tracks of C1 and MoSeN coatings are shown in Fig. 7c. The tracks were smooth with some vestiges of abrasion marks. Overall, the tracks were well covered with homogeneous tribolayer with no signs of delamination or underlayer exposures. This means the sliding occurred within the outer coating regime. The width of the wear track for C1 coating was slightly higher than those of MoSeN coatings.

3.3.5. Sliding in dry-N_2 atmosphere at 100 °C

The steady-state COF of coatings after dry-N_2 100 °C sliding are presented in Fig. 8a. The C1 coating displayed an average COF of ~0.065, a value not significantly different from the values observed at 100 °C when sliding under ambient atmosphere conditions. The addition of N produced similar results for the C2 and C3 coatings to the room temperature dry-N_2 tests, with COF values of ~0.028 and ~0.03, respectively. The C4 coating showed a slight increase in COF, reaching ~0.055. For this coating, the COF value increased gradually, so the average value was calculated from 400 seconds onwards.

The W*R* results presented in Fig. 8b show that the C1 coating

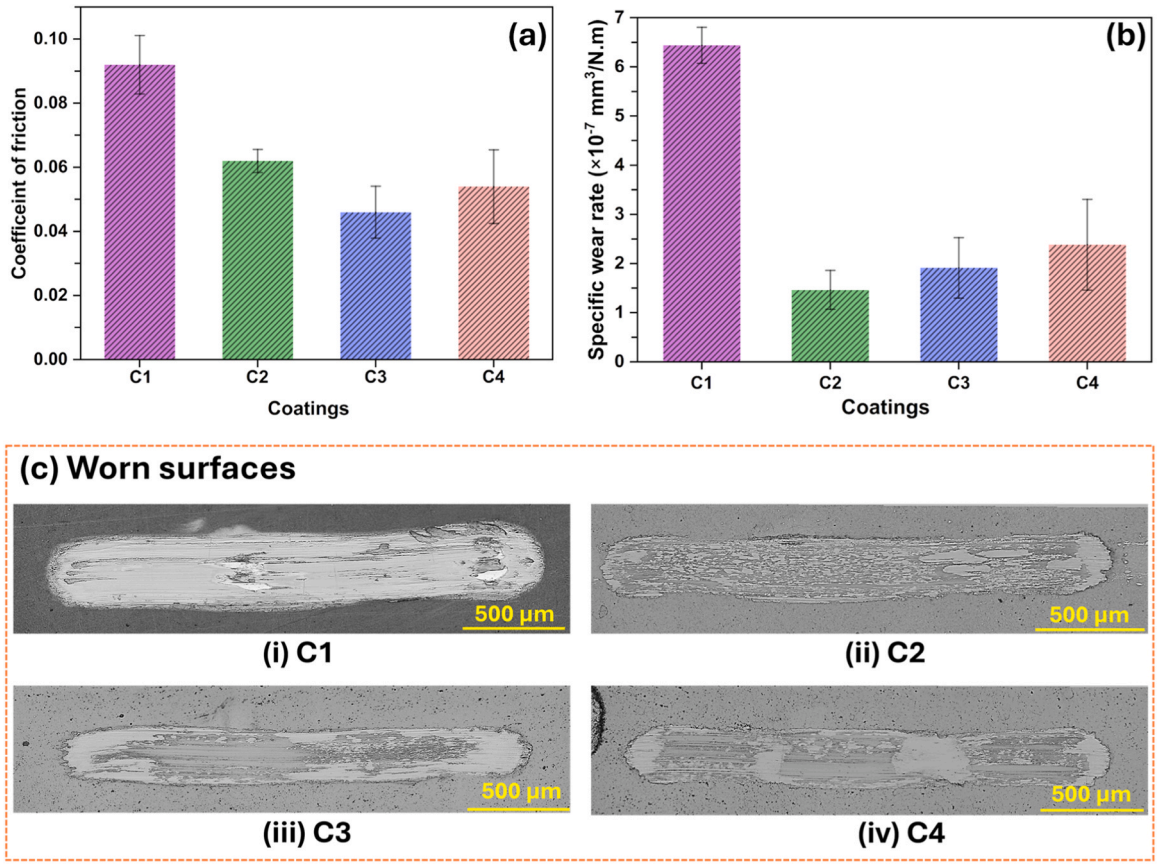

Fig. 5. (a) Friction coefficients, (b) Specific wear rates, and (c) Optical images of worn tracks of MoSeN coatings in ambient air at 100 °C.

exhibited a *WR* of 4.2×10^{-7} mm^3/Nm. The *WR* showed a substantial increase with the addition of 22 at% N (C2 coating). However, as the N content further increased, the *WR* decreased, with coatings C3 and C4 exhibiting values of 9×10^{-7} mm^3/Nm and 4.5×10^{-7} mm^3/Nm, respectively. Compared to the previously discussed conditions, these are the highest wear values measured for the C2 and C3 coatings.

The wear tracks of the pure $MoSe_2$ and MoSeN coatings, as shown in Fig. 8c, reveal clear signs of delamination for the C1, C2, and C3 coatings. This delamination became more pronounced with increasing nitrogen content, especially after 22 and 35 at% N alloying. Significant portions of these C3 and C4 coatings were delaminated, resulting in an abrupt increase in *WR*. The extensive delamination suggests that the coatings struggled to maintain their adhesion and structural integrity under these conditions, resulting in their compromised wear resistance and the subsequent increase in *WR*. Lastly, the C4 coating displayed less delamination, in agreement with the *WR* values.

3.3.6. *Sliding in dry-N_2 atmosphere at 200 °C*

The steady-state COF results for all coatings after sliding in dry-N_2 at 200 °C, are presented in Fig. 9. Due to the degraded coating performance, the test duration was reduced to 600 seconds to prevent complete failure of the coatings. Thus, like the tests conducted at 200 °C in ambient air, the coatings showed reduced performance with noticeable instability in both COF and *WR*. Overall, the current environment had the most detrimental implications on the tribological performance of coatings, as it significantly reduced their ability to maintain consistent friction and wear behaviour compared to all other testing conditions in this study.

For the C1 coating, the COF remained relatively stable above ~0.06 between 20 and 240 seconds, after which a gradual decrease was observed until about 450 seconds, followed by sharp spikes in the COF. The average COF, calculated from the stable region between 20 and 240 seconds, was ~0.065. In the case of the C2 coating, the average COF was determined from the first 200 seconds, during which the COF showed considerable fluctuations, before decreasing steadily up to 300 seconds. After that, strong fluctuations were observed. For the C3 coating, the COF fluctuated between ~0.05 and ~0.07 from 200 to 500 seconds, followed by a continuous decline with no noticeable spikes throughout the test. For the C4 coating, which had the highest N-alloying, the COF value fluctuated between 50 and 400 seconds, and then decreased continuously. The average COF value during this period was ~0.078 and no significant spikes were observed throughout the test.

Similar to the COF results, the wear performance of the coatings at 200 °C was notably inferior compared to the other test conditions. The C1 coating exhibited the maximum *WR* of 16.5×10^{-7} mm^3/Nm. As N content increased, a steady reduction in the wear was observed. The *WR* for the C2, C3, and C4 coatings were 15.8×10^{-7} mm^3 /Nm, 12.3×10^{-7} mm^3 /Nm, and 12.01×10^{-7} mm^3 /Nm, respectively. Despite the slight improvements with N-alloying, all wear tracks showed gross delamination and exposure of the underlayers; thus, they have not been shown here.

4. Discussion of results

4.1. *Fundamental characteristics of Coatings*

In C1 coating, the observed porosity and columnar morphology align well with the existing literature on sputtered TMD coatings. However, the degree of porosity and type of surface morphology differ from those reported for coatings with similar stoichiometry [25,60]. Most pure sputtered TMD coatings in literature exhibit a sponge-like morphology, whereas the morphology observed in this study is notably more compact (see Fig. 2a). This enhanced compactness is likely due to higher ad-atom mobility and reduced shadowing effect during deposition- this is

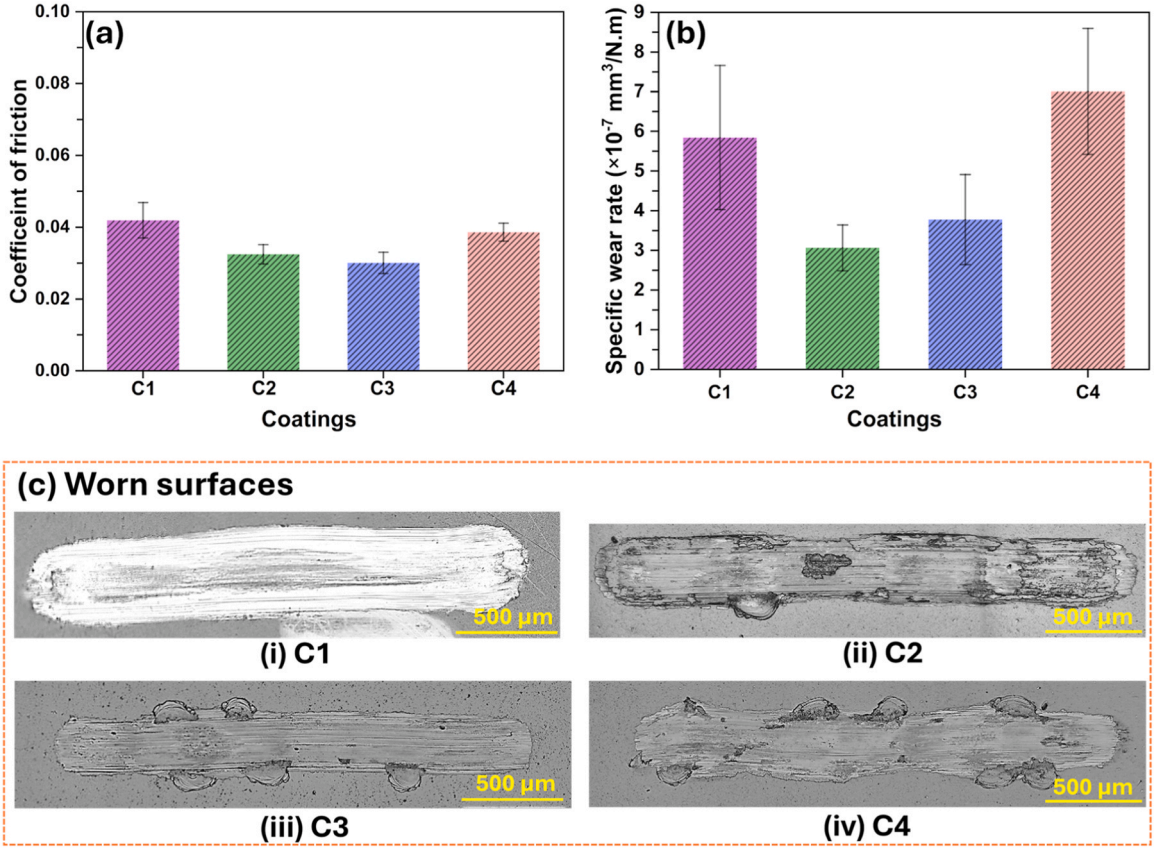

Fig. 6. (a) Friction coefficients, (b) Specific wear rates, and (c) Optical images of worn tracks of MoSeN coatings in ambient air at 200 °C.

attributed due to increased bombardment of back-scattered Ar neutrals and Ar+ ions [61]. For MoSeN coatings, enhanced compactness (see Fig. 2b) is attributed to the N coupled with surface limited growth conditions, again due to enhanced ad-atom mobility and Ar+ ions bombardment. In literature, sometimes even after adding N to pure TMD coating, the columnar morphology still persists, which is not the case here due to the use of substrate bias [57,62]. The use of substrate bias causes an increased/intense bombarding by Ar+ ions, which hit the growing coating, consequently decreasing impurities, voids and enhanced atomic coverage [63]. This increased compactness of TMD based coatings is favourable in achieving higher adhesion, mechanical strength, resistance to environmental attacks and resistance to wear [26,64–68].

For the chemical composition results (Fig. 2c), in pure coating (C1), the factors such as scattering of chalcogen atom in the chamber and re-sputtering of chalcogen atom from coating, which act as hindrances in achieving stoichiometric TMD coatings deposited via PVD sputtering are not playing any part here and have been overcome. This benefit is attributed to the lower mass difference between Mo and Se, unlike W and S or Mo and S, where the mass difference is quite high. Although some minor re-sputtering of Se may still occur due to the substrate bias, Ar+ ions, and reflected Ar neutrals. Nevertheless, this effect is mitigated by the minimal mass difference between Mo and Se, which preserves the integrity of the growing film [69,70]. This means that the rate of re-sputtering of both elements is similar, causing a uniform distribution of their contents in the deposited coating. For the MoSeN coatings, the results and trends achieved can be interpreted such that the values of the Se/Mo ratio are not actual representation of the $MoSe_2$ compound. In fact, a different mechanism is occurring and there are complexities involved in understanding the actual process of the role of N in TMD coatings. This is interpreted from the fact that the decrease in Se is quite huge as compared to the decrease in Mo and increase in N (as shown in Table S1). For C2 coating, N increased 21 at%, Mo decreased 4 at% and Se decreased 17 at%, indicating that N has a greater influence on Se content than on Mo. Similar trends have been observed for other coatings. Thus, the trends can be explained by combined effect of following phenomenon: -

- The measured values are for individual elements and not compounds.
- N replaces Se in the $MoSe_2$ compound. This results in the formation and presence of both Mo-N and some intermediary Mo-Se-N bonds/compounds [54].
- Some N occupies interstitial sites, while some N atoms may become trapped between $MoSe_2$ lamellae, as reported in ref [71].
- Re-sputtering of Se from growing coating by i) bombardment of Ar+ ions due to applied substrate bias [63,72] and ii) atoms arriving to substrate during coating deposition also reduces Se and creates possibilities of Mo combining with N.
- Overall, Se/Mo ratio in reality is thus slightly more than the one calculated from individual elemental concentration observed in WDS. This is a beneficial aspect with respect to tribology and sliding properties.

The crystal structure of the pure coating revealed a prominent peak pertaining to (002) basal planes almost parallel to the coating surface (see Fig. 2d). In TMDs, the easy shear properties, which are crucial for low-friction, are governed by these (002) planes [45,73]. Notably, the (002) orientation was more pronounced (with higher peak intensity) than that of the (10 L) orientation. This phenomenon can be attributed to the increased ion impingement on the growing coatings, favoured by the substrate bias, which enhances ad-atom mobility and promotes a more favourable crystallographic orientation towards the (002) plane. Moreover, Muratore et al. [74] reported that if deposition rate of TMD

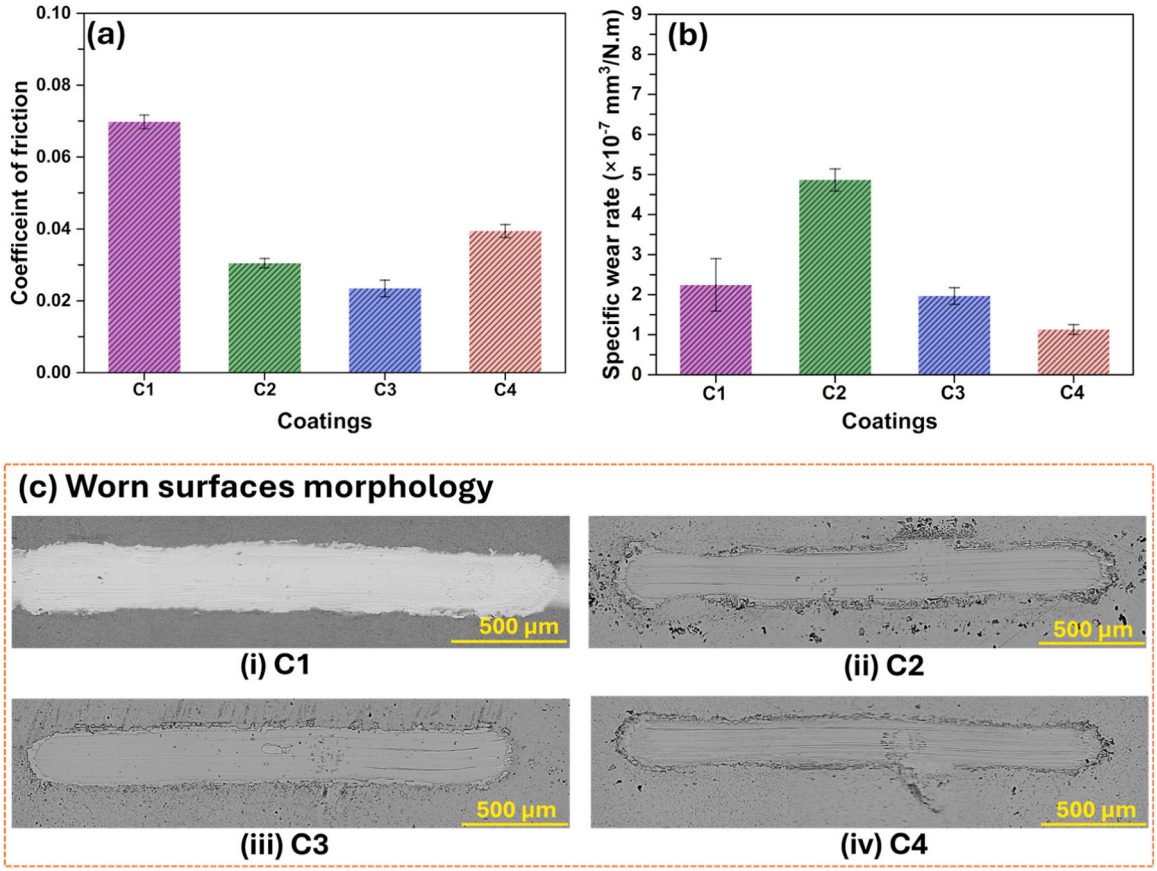

Fig. 7. (a) Friction coefficients, (b) Specific wear rates, and (c) Optical images of worn tracks of MoSeN coatings in dry-N_2 atmosphere at room temperature.

coating is close to 15 nm/min, the (002) preferential orientation is achieved. Moreover, despite the lower desorption energies of the (002) planes than the (100) planes, this can be favoured by energetic ions bombardment (Ar+ ions). Further, it was explained that a 15 nm/min deposition rate results in an increase in the burial rate of 2nd layer in comparison to the rate of desorption of the 1st layer, enhancing the contribution of the (002) orientation. It is to be noted that the deposition rate of C1coating achieved in our case was ~16 nm/min. For MoSeN coatings, the broad peak observed in ~30 – 50° range shows the presence of $MoSe_2$ crystals. Basically, XRD has limitations for analysis of crystals that are < 5 nm in size. From HRTEM analysis performed in previous studies [41,63], similar broad peaks were observed in this range when TMD platelets crystal size decreased to ~ 5 nm after alloying. Therefore, similar to the impact of C [41], incorporation of N in the coatings disturbs the growth and structural integrity of the crystals, leading to this smaller size, making coatings nanocrystalline.

The hardness results of the C1 coating shown in Fig. 3a are comparable to previously reported values for DCMS $MoSe_2$ coatings studied by the current authors [63], and it is slightly higher than the hardness values found in the literature for WS_2, MoS_2, and HiTUS sputtered $MoSe_2$ coatings [25,54,57]. This increment is attributed to the relatively compact morphology of the C1 coating in the present case, as compared to those reported in the literature [25,54,57]. Following the general trend that higher compactness and amorphousness correlate with higher hardness in alloyed TMD coatings, the hardness was further increased by the N-alloying. In addition, the potential Mo-N bonds presence and the reduction in crystallite sizes may also contribute to this increased hardness [54,75,76]. The hardness values obtained in this study are consistent with those of previously optimized MoSeC coatings deposited by DC and RF magnetron sputtering, making them suitable for efficient tribological performance [63].

4.2. Tribological results

4.2.1. Ambient air tests

The sliding property of the coating in a room temperature environment can be explained based on the fundamental characteristics of deposited coatings. The C1 coating is porous and exhibits columnar morphology with voids, making it more susceptible to environmental factors, particularly moisture [30]. Thus, the COF is the highest at room temperature ambient air conditions. Overall, this COF is still better than our recently reported Mo-Se-C and W-S-N coatings [30,41,44,45] while, slightly more than HiTUS sputtered MoSeN coatings [54]. The lower wear rate observed for the C1 coating, compared to all MoSeN coatings, is attributed to: (i) its highest Se/Mo stoichiometry, which is always the most desirable parameter in TMD coatings. A higher the stoichiometry facilitates a more robust tribo-layer formation [26,55–57], leading to rapid wear track coverage; (ii) the presence of the (002) preferential orientation (see Fig. 2d), which further enhances sliding properties; and (iii) the soft nature of pure coating, which promotes efficient tribolayer formation and wear track coverage. Moreover, in TMDs, after an initial period of wear, the worn material becomes trapped between the sliding surfaces and acts as a third body that gradually covers the entire wear track. This mechanism of tribolayer formation is described in detail in our previous work [73]. With N additions, the coatings became dense and compact, as shown in Fig. 2b, removing porosity and susceptibility to environmental attacks, leading to less degradation of COF. Similar COF by all MoSeN coatings is related to the fact that coatings have sufficiently become compact to sustain the environmental impacts. Similarly, as explained in compositional results, some of the N is bonded to Mo and there is sufficient $MoSe_2$ available in coatings to form the easy shear tribolayer. This consistent sliding performance with variations of N content is a promising result as it overcomes the compositional variations impact caused during PVD sputtering of 3D parts, as briefly

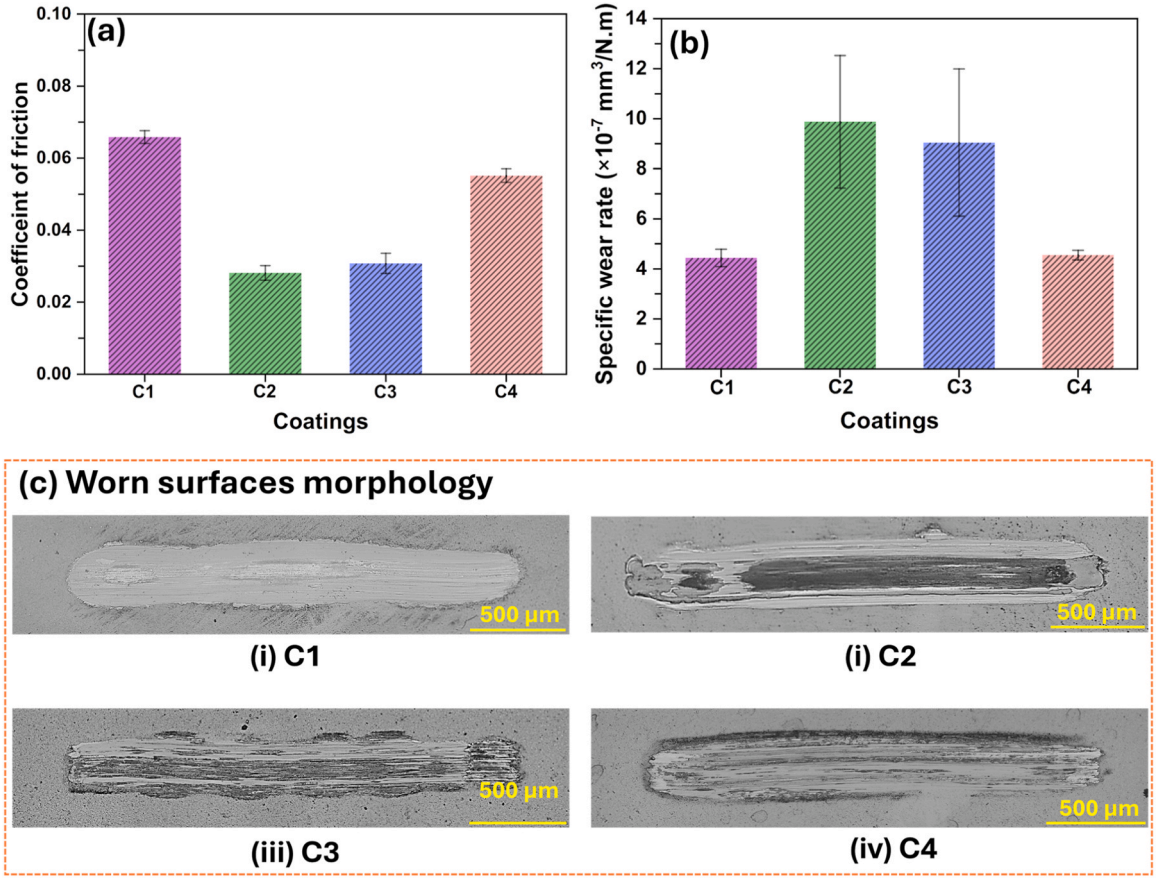

Fig. 8. (a) Friction coefficients, (b) Specific wear rates, and (c) Optical images of worn tracks of MoSeN coatings in dry-N_2 atmosphere at 100 °C.

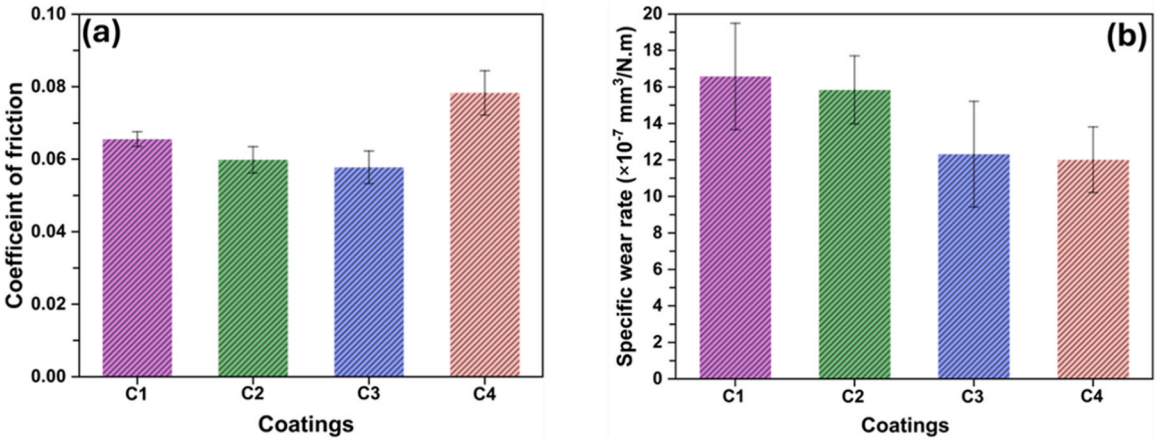

Fig. 9. (a) Friction coefficients, and (b) Specific wear rates of MoSeN coatings in dry-N_2 atmosphere at 200 °C.

reported in our previous work [43]. The slightly increased wear of MoSeN coatings as compared to the C1 coating is because there is always some wear required to form the tribolayer and after N alloying, the required amount of wear is slightly higher to overcome the effect of reduced Se/Mo ratio. Once sufficient $MoSe_2$ is available, the tribolayer forms and supports continued sliding. Similar to the COF, the W*R* results are consistent for all N-alloyed coatings, providing a competitive edge over other alloyed TMD coatings in addressing the inherent limitations of the PVD deposition process.

At 100 °C, the C1 coating exhibited a higher COF due to its porous morphology and greater susceptibility to high-temperature oxidation (Fig. 5a). This instability during sliding resulted in the exposure of the underlayer within the wear tracks (Fig. 5c), which in turn led to increased W*R*. The exposure of the underlayer also hindered the formation of an effective shear tribolayer of $MoSe_2$, and the lack of a uniform tribolayer contributed to the high COF. In contrast, the MoSeN coatings showed no evidence of underlayer exposure, demonstrating enhanced stability, which is reflected in lower W*R* (Fig. 5b). Thus, N incorporation effectively mitigated the effects of environmental degradation, particularly the oxidation of TMDs. If related to the basic properties of coatings, the increased compactness and slightly less Se/Mo ratio after N alloying were the contributing factors for this stable behaviour. Overall, in MoSeN coatings, the increased of temperature to 100 °C had a minimal impact on COF, as the coatings maintained similar

values. However, there was a slight improvement in wear performance, highlighting the benefits of N incorporation in enhancing the thermal stability and durability of coatings.

At 200 °C, the lowest COF obtained among all tests in ambient air is attributed to the temperature induced easy sliding of the TMD layers (Fig. 6a). TMDs upon exposure to high temperatures can get oxidized, which enhances their wear and exfoliation but at the same time, temperature can increase re-orientation of the easy shear tribolayers. Moreover, temperature also removes the moisture, which, if present, has adverse effects on the sliding properties [52,77]. The exfoliation and possible oxidation at high temperatures is the reason why coatings showed delaminated zones and increased wear [77]. The reason for increased wear with N increments (Fig. 6b) can only be related to the fact that the sufficient compromise between the formation of an easy shear layer and exfoliation could not be achieved in a way that the coating could resist delamination (Fig. 6c) i.e., less $MoSe_2$ was available to form the layer capable of covering the wear track. Additionally, the formation of hard Mo and Fe oxides (with Fe coming from the steel counterpart) could contribute to increased wear, as these hard particles can damage the wear tracks when interacting with softer coatings. This possibility presents an intriguing avenue for future exploration.

4.2.2. *Dry-N_2 tests*

For the tests performed in room temperature conditions, the comparatively lower COF of all coatings is due to the absence of moisture and humidity (Fig. 7a). This dry atmosphere supports the rapid and efficient tribolayer formation, in agreement with the fact that TMD coatings display superior sliding properties in the dry atmosphere [27,37]. Overall, the difference between all MoSeN coatings is not significant in our system due to two reasons: i) $MoSe_2$ is that subset of TMDs which is known for its excellent sliding properties even in ambient air, particularly when compared to MoS_2 or WS_2 [30], ii) the coatings were sufficiently compact to withstand the effects of environmental degradation even in ambient air sliding. In fact, the slight increment of COF of C4 coating is directly linked to less availability of $MoSe_2$ compound in the coating and consequently in the contact. In relation to the achieved promising W*R* performance, again the dry sliding environment supported the sliding performance as compared to ambient air tests. Here, the C2 coating's W*R* was higher as the observed the wear track depth was also higher than other coatings (e.g., 0.98 μm for C2 vs 0.2 μm for C4 coating).

At 100 °C, the COF observed for C1, C2 and C3 coating is again related to the absence of humidity and enhanced easy shear properties with temperature. However, the C4 coating exhibits a slight anomaly as the increase in COF does not align with the trends observed in the other coatings (Fig. 8a). This increase is due to delayed availability of the easy shear layer, resulting from lower wear (Fig. 8b). The W*R* for the C1 coating increased as compared to the room temperature, primarily due to greater degradation from the elevated temperature as supported by the wear track images showing signs of delamination (Fig. 8c). Similarly, the increased W*R* for the C2 and C3 coatings is linked to the delamination caused by exfoliation at higher temperatures, a phenomenon that is more pronounced in dry-N_2 100 °C than 100 °C ambient air. In this case, basically all thermal energy is directly impacting exfoliation, while no thermal energy is being consumed to remove moisture. The low wear observed in the C4 coating, in combination with its high COF, suggests a correlation between these two factors. This coating has the lowest Se/Mo ratio and it is slightly more compact than coatings with a lower N content, allowing it to be more resistant to thermal degradation, which results in a lower W*R* but increased COF. This behaviour is consistent with findings in the literature, indicating that a longer duration of sliding is required for the coating with more alloying content and a low ratio to achieve a stable COF, as described in the literature [30].

In the final testing condition, which involved sliding in dry-N_2 at 200 °C, both COF and the wear properties were poorer than those observed in all other atmospheres (Fig. 9). In ambient air at 200 °C, it was observed that the coatings displayed adverse properties, and a similar trend was observed here with further degradation in the properties. Notably, the C1 and C2 coatings, in particular, struggled to sustain smooth sliding for even 600 seconds. Although it is seen from the graphs that the COF is not significantly high, it cannot be ignored that the COF was never stable. Likewise, the W*R* under these conditions were the worst compared to all other atmospheres, with wear tracks showing significant damage and exposure of the underlying layers. This decline in performance can be directly attributed to the high-temperature exfoliation of these coatings, which compromised their structural integrity and overall sliding efficiency. From 100 °C it was concluded that all thermal energy is being used in the exfoliation as none was required for the moisture removal (as was seen in ambient air tests). Thus, the effect of temperature being pronounced on delamination relates to this observation.

4.2.3. *High temperature oxidation and Raman analysis of wear track*

This section is dedicated to the discussion of the two important aspects that contribute to the sliding efficiency of coatings in this study. First is the role of tribolayer formation due to reorientation and transfer layer mechanism reported in ref [45]. To investigate and ensure this tribo-induced structural changes of $MoSe_2$ in the wear tracks, one wear track was selected for Raman intensity map of E^1_{2g} peak in the spectral range of 255 – 330 cm^{-1} (Fig. 10a) for two different regions namely, i) point 1 and ii) point 2 were analysed. The achieved results of Raman intensity mapping show that both regions depict distinct crystallinity, the red zone being more crystalline than the blue zone. Moreover, the spectra presented in Fig. 10c also clarifies that no well-defined crystalline $MoSe_2$ peaks were detected in the point 1 and it displayed results similar to the as-deposited coating. On the other hand, the point 2 displayed well defined crystalline peaks, depicting the formation of easy shear $MoSe_2$ tribolayer. Thus, tribo induced $MoSe_2$ easy shear layers formation due to reorientation and transfer layer mechanisms, similar to the one reported in ref[73], are responsible for the low friction.

Similarly, the second crucial part of this section deals with the investigation of the impact of temperature on the degradation of coatings. One MoSeN coating was selected and exposed to a high temperature of 400 °C. This temperature was chosen to accelerate the effects of thermal exposure beyond the previously tested limit of 200 °C. Post-mortem analysis of the exposed coating was carried out using SEM. As can be seen in Fig. 11a, the surface morphology revealed the formation of bubbles and cracks, while the previously observed cauliflower-like features began to disappear. Cross-sectional micrographs (Fig. 10b) illustrated noticeable cracking and exfoliation of the coatings in layered formations. These observations confirm that the coating undergoes cracking and detachment from the substrate in layers due to enhanced exfoliation effects induced by elevated temperatures (see similar effects of degradation with increasing temperature in ref [77]). To further examine this effect of temperature on coating oxidation, in-situ XRD was performed at room temperature and 400 °C. The XRD results presented in Fig. 11c clearly demonstrate the presence of well intense Mo-O peaks, further ensuring the degradation of coatings with temperature. Thus, the best working limit of MoSeN coatings remains up to 100 °C in ambient air and dry-N_2 with COF and W*R* values very close to each other. 200 °C in ambient air can also work, but delamination factors must be kept in mind and maybe overcome, if possible.

5. Conclusions

To explore the potential of MoSeN coatings in providing promising sliding properties in diverse sliding environmental conditions, and at the same time overcoming the inherent issues faced in PVD sputtering in relation to composition/property variations, DCMS sputtered MoSeN coatings were the focus of this research. The coatings with N-alloying of 21 – 42 at% displayed consistent properties in regards to their morphology, compactness, structure and hardness. The sliding

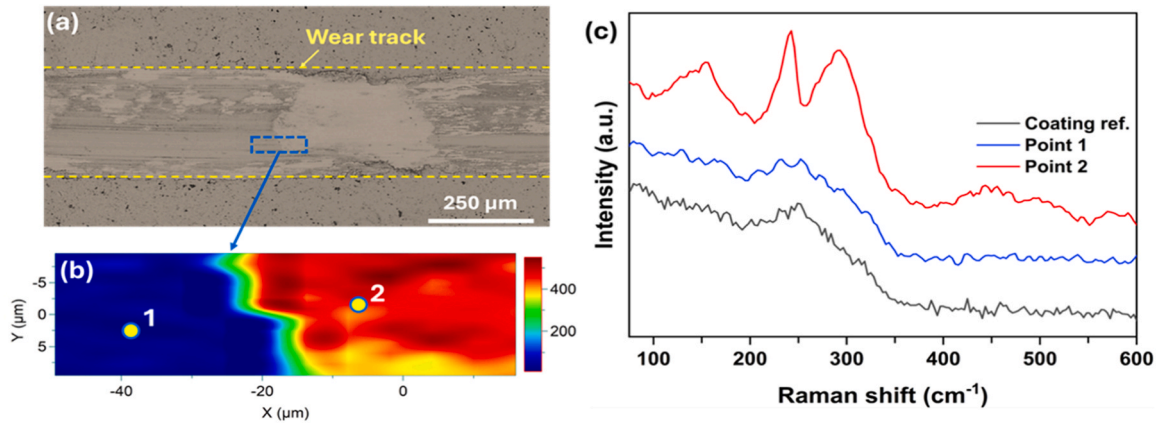

Fig. 10. Raman analysis of the worn region inside the wear track - (a) Optical image of the wear track on MoSeN coating, (b) Raman intensity map of the E^1_{2g} peak in the spectral range of 255 – 330 cm^{-1}, and (c) Corresponding Raman spectra of the coating and the points marked in (b).

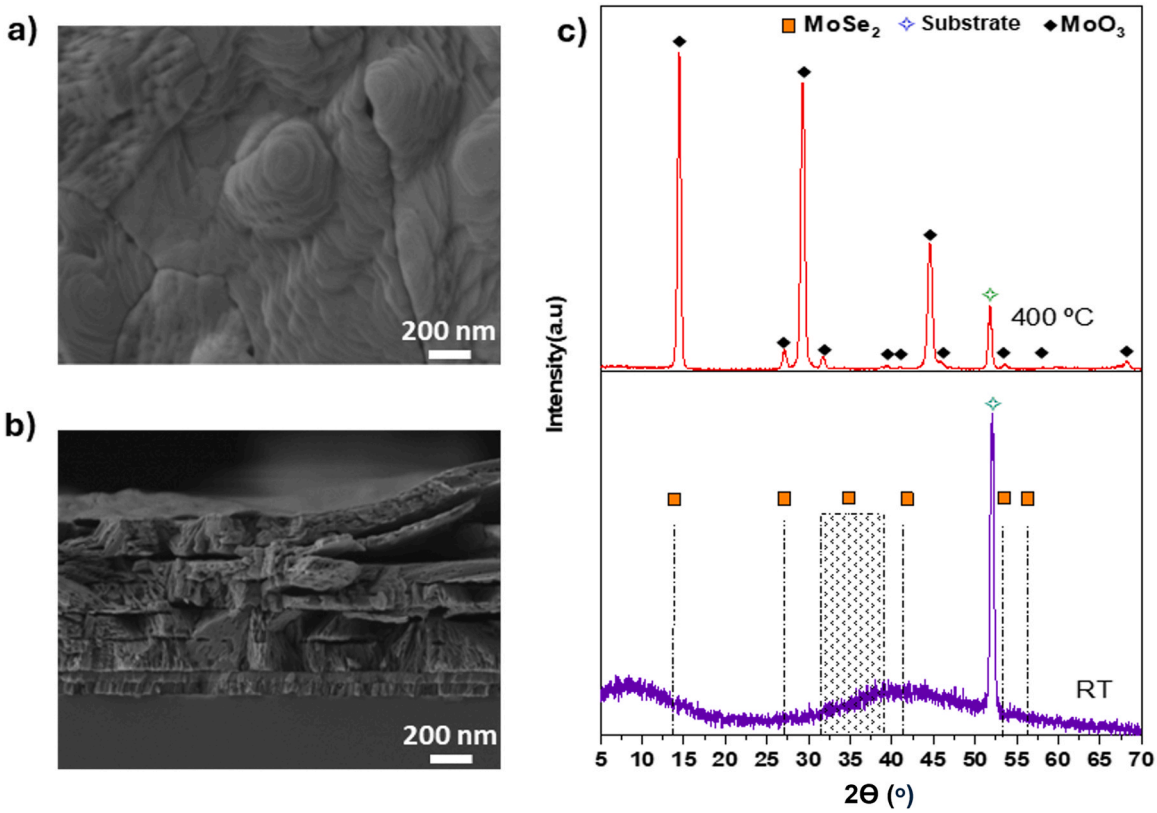

Fig. 11. (a) Surface morphology, and (b) Cross-sectional morphology micrographs obtained after 400 °C exposed MoSeN coating, and (c) In-situ hot XRD pattern of MoSeN coating at RT and 400 °C.

efficiency was rigorously studied in six different sliding conditions. The main conclusions drawn from these sliding tests are as follows:

a. Introducing N in the coatings enhances their compactness and hardness. The Se/Mo ratio calculated from individual elemental composition displayed a decrease with increasing N content.
b. The crystal structure became amorphous with N additions, showing a broad peak in ~30 – 50° region, suggesting the presence of $MoSe_2$ nanocrystals with less than 5 nm size.
c. All N alloyed coatings displayed consistent morphology, crystal structure and hardness, irrespective of N variations from 21 – 42 at %.
d. In relation to COF, the achieved results for N alloyed coatings were always superior to the C1 $MoSe_2$ coatings owing to their enhanced compactness, mechanical properties and resistance to environmental impacts. In all conditions except dry-N_2 100 °C and dry-N_2 200 °C, the maximum COF difference among different coatings sliding within each specific environmental condition was 0.01 – 0.02, which is within the error range so can be ignored. Even in dry-N_2 100 °C, the only coating displaying slightly higher COF was the highest N containing coating. Similarly, in all the environments combined (except dry-N_2 100 °C and dry-N_2 200 °C), the global COF variations lied between 0.03 and 0.06, a range much smaller when compared to the diverse environment sliding properties of other alloyed TMD coatings reported in literature.

e. The *WR* variations of N-containing coatings, in above mentioned conditions, were small, lying in the range of 1–7 $\times$ 10^{-7} mm^3/Nm.
f. At 200 °C, the coatings were found to exfoliate in layered form, leading to a degraded wear performance and exposing the underlying substrate.

Overall, this study represents the first comprehensive investigation into the performance of DCMS sputtered MoSeN coatings for sliding applications across diverse environments. It emphasizes that despite the compositional fluctuations often encountered during the PVD coating of complex 3D parts, these coatings exhibit promising sliding characteristics up to 100 °C. To enable efficient sliding at 200 °C, further optimization will be essential. Consequently, the scaling up of these coatings for industrial applications, particularly in mobility sectors where energy conservation and environmentally friendly solutions are paramount, is strongly recommended.

Statement of originality

The authors confirm that the manuscript is original and is the sole work of the main and co-authors. This article has never been submitted or published in any other journal.

CRediT authorship contribution statement

Talha Bin yaqub: Writing – review & editing, Writing – original draft, Visualization, Validation, Methodology, Investigation, Formal analysis, Data curation, Conceptualization. **Irfan Nadeem:** Writing – original draft, Software, Formal analysis, Data curation. **Filipe Fernandes:** Methodology, Formal analysis, Data curation. **Khurram Yaqoob:** Writing – original draft, Visualization. **Mitjan Kalin:** Supervision, Resources, Funding acquisition, Project administration, Writing – review & editing. **Albano Cavaleiro:** Writing – review & editing, Validation, Supervision, Resources, Project administration, Funding acquisition.

Declaration of Competing Interest

The authors declare that they have no known competing financial interests or personal relationships that could have appeared to influence the work reported in this paper.

Acknowledgements

The authors acknowledge the funding for this research by the Slovenian Research Agency ARIS under the Research Core Funding Programme No. P2-0231 and Marie-Sklodowska Curie COFUND—Seal of Excellence No. 5100-237/2023-7 (5 February 2024). The work is also sponsored by national funds through FCT—Fundação para a Ciência e a Tecnologia, under projects UID/00285—Centre for Mechanical Engineering, Materials and Processes and LA/P/0112/2020.

Appendix A. Supporting information

Supplementary data associated with this article can be found in the online version at doi:10.1016/j.triboint.2025.110716.

Data availability

Data will be made available on request.

References

[1] Zia AW, Hussain SA, Baig MMFA. Optimizing diamond-like carbon coatings - from experimental era to artificial intelligence. Ceram Int 2022;48:36000–11. https://doi.org/10.1016/j.ceramint.2022.10.149.
Ciulli E., Quaglia G., Gasparetto A., Petuya V., Carbone G. Tribology and Sustainable Development Goals. Springer International Publishing; 2022. p. 438–447.
[3] Huck W. Sustainable Development Goals. Cambridge University Press; 2022. https://doi.org/10.5771/9783748902065.
[4] Tzanakis I, Hadfield M, Thomas B, Noya SM, Henshaw I, Austen S. Future perspectives on sustainable tribology. Renew Sustain Energy Rev 2012;16:4126–40. https://doi.org/10.1016/j.rser.2012.02.064.
[5] Fiorino DJ. The New Environmental Regulation. MIT Press; 2006.
[6] Berman D, Farfan-Cabrera LI, Rosenkranz A, Erdemir A. Advancing the frontiers of EV tribology with 2D materials – a critical perspective. Mater Sci Eng R: Rep 2024;161:100855. https://doi.org/10.1016/j.mser.2024.100855.
[7] Berman D, Mutyala KC, Srinivasan S, Sankaranarayanan SKRS, Erdemir A, Shevchenko EV, Sumant AV. Iron-nanoparticle driven tribochemistry leading to superlubric sliding interfaces. Adv Mater Interfaces 2019;6:1–8. https://doi.org/10.1002/admi.201901416.
[8] Nadeem I, Ambrožič B, Dražić G, Kovač J, Cavaleiro A, Kalin M. Super-low friction and wear in steel contacts enabled by tribo-induced structural degradation of graphene quantum dots. Mater Des 2024;244. https://doi.org/10.1016/j.matdes.2024.113111.
[9] Nadeem I, Malok M, Kovač J, Bin Yaqub T, Cavaleiro A, Kalin M. Superior macroscale tribological performance of steel contacts based on graphene quantum dots in aqueous glycerol. Tribol Int 2023;181. https://doi.org/10.1016/j.triboint.2023.108328.
[10] Fitch EC. Fluid Chemical Stability. Proactive Maintenance for Mechanical Systems. Elsevier; 1992. p. 99–126. https://doi.org/10.1016/B978-1-85617-166-3.50005-6.
[11] Technical Committee of Petroleum. Additive Manufacturers in Europe. Lubricant Additives and the Environment. Atc 2007:49.
[12] Vetter J. Surface Treatments for Automotive Applications. Coating Technology for Vehicle Applications (book). Springer; 2015. p. 91–132.
[13] Lansdown AR. Molybdenum disulphide lubrication. Elsevier; 1999.
[14] Nadeem I, Akhter R, Akhtar S, Tauqir A. Optimization of pulsed fiber laser texturing for solid lubricant deposition on a Ti/TiN coated aerospace alloy. Advanced Materials - XVI, 875. Trans Tech Publications Ltd; 2021. p. 337–45. https://doi.org/10.4028/www.scientific.net/KEM.875.337.
[15] Liu Y, Fan Z, Yu S, Zhang R, Zhang J, Liskiewicz TW, et al. Macroscale structural superlubricity: dynamic evolution of tribolayers in two-dimensional materials under extreme pressure. Nano Energy 2024;129. https://doi.org/10.1016/j.nanoen.2024.110072.
[16] Teer DG. New solid lubricant coatings. Wear 2001;251:1068–74. https://doi.org/10.1016/S0043-1648(01)00764-5.
[17] Voevodin AA, Zabinski JS. Nanocomposite and nanostructured tribological materials for space applications. Compos Sci Technol 2005;65:741–8. https://doi.org/10.1016/j.compscitech.2004.10.008.
[18] Roberts EW. Thin solid lubricant films in space. Tribol Int 1990;23(2):95–104. https://doi.org/10.1016/0301-679X(90)90042-N.
[19] Scharf TW, Prasad SV. Solid lubricants: a review. J Mater Sci 2013;48:511–31. https://doi.org/10.1007/s10853-012-7038-2.
[20] Grill A. Diamond-like carbon: state of the art. Diam Relat Mater 1999;8:428–34. https://doi.org/10.1016/S0925-9635(98)00262-3.
[21] Esteve J, Zambrano G, Rincon C, Martinez E, Galindo H, Prieto P. Mechanical and tribological properties of tungsten carbide sputtered coatings. Thin Solid Films 2000;373:282–6. https://doi.org/10.1016/S0040-6090(00)01108-1.
[22] Ji L, Li H, Zhao F, Chen J, Zhou H. Microstructure and mechanical properties of Mo/DLC nanocomposite films. Diam Relat Mater 2008;17:1949–54. https://doi.org/10.1016/J.DIAMOND.2008.04.018.
[23] Dai MJ, Wei CB, Zhou KS, Zhu M, Hou HJ, Lin SS, et al. Properties of W/DLC/W-S-C composite films fabricated by magnetron sputtering. Trans Nonferrous Met Soc China (Engl Ed) 2015;25:3002–11. https://doi.org/10.1016/S1003-6326(15)63927-9.
[24] Prasad SV, Zabinski JS. Tribology of tungsten disulphide (WS2): characterization of wear-induced transfer films. J Mater Sci Lett 1993;12:1413–5. https://doi.org/10.1007/BF00591592.
[25] Polcar T, Cavaleiro A. Review on self-lubricant transition metal dichalcogenide nanocomposite coatings alloyed with carbon. Surf Coat Technol 2011;206:686–95. https://doi.org/10.1016/j.surfcoat.2011.03.004.
[26] Polcar T, Cavaleiro A. Self-adaptive low friction coatings based on transition metal dichalcogenides. Thin Solid Films 2011;519:4037–44. https://doi.org/10.1016/j.tsf.2011.01.180.
[27] Yaqub T.Bin Optimization Of Sputtered Mo-Se-C Coatings For Efficient Self-adaptation During Sliding In Diverse Environments 2020.
[28] Erdemir A, Bhushan B. Modern Tribology Handbook. CRC Press; 2001.
[29] Myshkin NK, Petrokovets MI, Kovalev AV. Tribology of polymers: Adhesion, friction, wear, and mass-transfer. Tribol Int 2005;38:910–21. https://doi.org/10.1016/j.triboint.2005.07.016.
[30] Yaqub TBin, Vuchkov T, Evaristo M, Cavaleiro A. DCMS Mo-Se-C solid lubricant coatings – synthesis, structural, mechanical and tribological property investigation. Surf Coat Technol 2019. https://doi.org/10.1016/j.surfcoat.2019.124992.
[31] Yaqub TBin, Hebbar Kannur K, Vuchkov T, Pupier C, Héau C, Cavaleiro A. Molybdenum diselenide coatings as universal dry lubricants for terrestrial and aerospace applications. Mater Lett 2020;275. https://doi.org/10.1016/j.matlet.2020.128035.
[32] Voevodin AA, O'Neill JP, Zabinski JS. Nanocomposite tribological coatings for aerospace applications. Surf Coat Technol, 116–119. Sequoia SA: Elsevier; 1999. p. 36–45. https://doi.org/10.1016/S0257-8972(99)00228-5.

[33] Rapoport L, Bilik Y, Feldman Y, Homyonfer M, Cohen SR, Tenne R. Hollow nanoparticles of WS2 as potential solid-state lubricants. Nature 1997;387:791–3. https://doi.org/10.1038/42910.

[34] Prasad S, Zabinski J. Super slippery solids. Nature 1997;387:761. https://doi.org/10.1038/42820.

[35] Liao M, Wei Z, Du L, Wang Q, Tang J, Yu H, et al. Precise control of the interlayer twist angle in large scale MoS2 homostructures. Nat Commun 2020;11:1–8. https://doi.org/10.1038/s41467-020-16056-4.

[36] Paradisanos I, Shree S, George A, Leisgang N, Robert C, Watanabe K, et al. Controlling interlayer excitons in MoS2 layers grown by chemical vapor deposition. Nat Commun 2020;11:1–7. https://doi.org/10.1038/s41467-020-16023-z.

[37] Kannur KH, Yaqub TBin, Pupier C, Héau C, Cavaleiro A. Mechanical properties and vacuum tribological performance of Mo-S-N sputtered coatings. ACS Appl Mater Interfaces 2020;12:43299–310. https://doi.org/10.1021/acsami.0c12655.

[38] Muratore C, Voevodin AA. Molybdenum disulfide as a lubricant and catalyst in adaptive nanocomposite coatings. Surf Coat Technol 2006;201:4125–30. https://doi.org/10.1016/j.surfcoat.2006.08.014.

[39] Shang K, Zheng S, Ren S, Pu J, He D, Liu S. Improving the tribological and corrosive properties of MoS 2 -based coatings by dual-doping and multilayer construction. Appl Surf Sci 2018;437:233–44. https://doi.org/10.1016/j.apsusc.2017.12.167.

[40] Abid T, Akram MA, Yaqub TBin, Ramzan Abdul Karim M, Fernandes F, Zafar MF, et al. Design and development of porous CoCrFeNiMn high entropy alloy (Cantor alloy) with outstanding electrochemical properties. J Alloy Compd 2024;970. https://doi.org/10.1016/j.jallcom.2023.172633.

[41] Vuchkov T, Yaqub TBin, Evaristo M, Cavaleiro A. Synthesis, microstructural and mechanical properties of self-lubricating Mo-Se-C coatings deposited by closed-field unbalanced magnetron sputtering. Surf Coat Technol 2020;394. https://doi.org/10.1016/j.surfcoat.2020.125889.

[42] Vuchkov T, Yaqub TBin, Evaristo M, Cavaleiro A. Synthesis, microstructural, and mechano-tribological properties of self-lubricatingw-s-c(h) thin films deposited by different RF magnetron sputtering procedures. Coatings 2020;10. https://doi.org/10.3390/coatings10030272.

[43] Yaqub TBin, Fernandes F, Al-Rjoub A, Cavaleiro A. Mo-Se-N dry lubricant coatings as a universal solution for protecting surfaces of complex 3D parts. Mater Lett 2022;316. https://doi.org/10.1016/j.matlet.2022.131967.

[44] Yaqub TBin, Al-Rjoub A, Cavaleiro A, Fernandes F. Exploring the industrial implementation of W–S–N coatings: a detailed study of the synthesis, compositional, structural, mechanical and multi-environment lubrication properties. J Mater Res Technol 2022;18:547–63. https://doi.org/10.1016/j.jmrt.2022.02.116.

[45] Yaqub TBin, Bruyere S, Pierson JF, Vuchkov T, Cavaleiro A. Insights into the wear track evolution with sliding cycles of carbon-alloyed transition metal dichalcogenide coatings. Surf Coat Technol 2020;403. https://doi.org/10.1016/j.surfcoat.2020.126360.

[46] Cao H, Wen F, Kumar S, Rudolf P, De Hosson JTM, Pei Y. On the S/W stoichiometry and triboperformance of WSxC(H) coatings deposited by magnetron sputtering. Surf Coat Technol 2019;365:41–51. https://doi.org/10.1016/j.surfcoat.2018.04.040.

[47] Takeno T, Abe S, Adachi K, Miki H, Takagi T. Deposition and structural analyses of molybdenum-disulfide (MoS2)-amorphous hydrogenated carbon (a-C:H) composite coatings. Diam Relat Mater 2010;19:548–52. https://doi.org/10.1016/j.diamond.2009.10.028.

[48] Zhang X, Qiao L, Chai L, Xu J, Shi L, Wang P. Structural, mechanical and tribological properties of Mo-S-N solid lubricant films. Surf Coat Technol 2016;296:185–91. https://doi.org/10.1016/j.surfcoat.2016.04.040.

[49] Polcar T, Nossa A, Evaristo M, Cavaleiro A. Nanocomposite coatings of carbon-based and transition metal dichalcogenides phases: A Review. Rev Adv Mater Sci 2007;15:118–26.

[50] Isaeva L, Sundberg J, Mukherjee S, Pelliccione CJ, Lindblad A, Segre CU, et al. Amorphous W-S-N thin films: the atomic structure behind ultra-low friction. Acta Mater 2015;82:84–93. https://doi.org/10.1016/j.actamat.2014.08.043.

[51] Sundberg J, Nyberg H, Särhammar E, Nyberg T, Jacobson S, Jansson U. Influence of composition, structure and testing atmosphere on the tribological performance of W-S-N coatings. Surf Coat Technol 2014;258:86–94. https://doi.org/10.1016/j.surfcoat.2014.09.061.

[52] Kubart T, Polcar T, Kopecký L, Novák R, Nováková D. Temperature dependence of tribological properties of MoS2 and MoSe2 coatings. Surf Coat Technol 2005;193:230–3. https://doi.org/10.1016/j.surfcoat.2004.08.146.

[53] Brainard WA. The thermal stability and friction of the disulfides, diselenides, and ditellurides of molybdenum and tungsten in vaccum (10-9 to 10-6 TORR). NASA Tech Note D-5141 1968:1–26.

[54] Hudec T, Izai V, Satrapinskyy L, Huminiuc T, Roch T, Gregor M, et al. Structure, mechanical and tribological properties of MoSe2 and Mo-Se-N solid lubricant coatings. Surf Coat Technol 2021;405. https://doi.org/10.1016/j.surfcoat.2020.126536.

[55] Vuchkov T, Evaristo M, Yaqub TBin, Cavaleiro A. The effect of substrate location on the composition, microstructure and mechano-tribological properties of W-S-C coatings deposited by magnetron sputtering. Surf Coat Technol 2020;386:125481. https://doi.org/10.1016/j.surfcoat.2020.125481.

[56] Weise G, Mattern N, Hermann H, Teresiak A, Bächer I, Brückner W, et al. Preparation, structure and properties of MoSx films. Thin Solid Films 1997;298:98–106. https://doi.org/10.1016/S0040-6090(96)09165-1.

[57] Kannur KH, Yaqub TBin, Huminiuc T, Polcar T, Pupier C, Héau C, et al. Synthesis and structural properties of Mo-S-N sputtered coatings. Appl Surf Sci 2020;527:146790. https://doi.org/10.1016/j.apsusc.2020.146790.

[58] Leyland A, Matthews A. On the significance of the H/E ratio in wear control: a nanocomposite coating approach to optimised tribological behaviour. Wear 2000;246:1–11. https://doi.org/10.1016/S0043-1648(00)00488-9.

[59] Musil J, Kunc F, Zeman H, Poláková H. Relationships between hardness, Young's modulus and elastic recovery in hard nanocomposite coatings. Surf Coat Technol 2002;154:304–13. https://doi.org/10.1016/S0257-8972(01)01714-5.

[60] Polcar T, Evaristo M, Cavaleiro A. Comparative study of the tribological behavior of self-lubricating W-S-C and Mo-Se-C sputtered coatings. Wear 2009;266:388–92. https://doi.org/10.1016/j.wear.2008.04.011.

[61] Särhammar E, Strandberg E, Sundberg J, Nyberg H, Kubart T, Jacobson S, et al. Mechanisms for compositional variations of coatings sputtered from a WS2 target. Surf Coat Technol 2014;252:186–90. https://doi.org/10.1016/j.surfcoat.2014.04.066.

[62] Nossa A, Cavaleiro A, Carvalho NJM, Kooi BJ, Hosson JTMDe. On the microstructure of tungsten disulfide films alloyed with carbon and nitrogen. Thin Solid Films 2005;484:389–95. https://doi.org/10.1016/j.tsf.2005.02.018.

[63] Yaqub TBin, Vuchkov T, Sanguino P, Polcar T, Cavaleiro A. Comparative study of DC and RF sputtered MoSe2 coatings containing carbon-an approach to optimize stoichiometry, microstructure, crystallinity and hardness. Coatings 2020;10. https://doi.org/10.3390/coatings10020133.

[64] Cao H, Hosson JTMDe, Pei Y. Self-healing of a pre-notched WS2/a-C coating. Mater Res Lett 2019;7:103–9. https://doi.org/10.1080/21663831.2018.1561538.

[65] Cao H, De Hosson JTM, Pei Y. Effect of carbon concentration and argon flow rate on the microstructure and triboperformance of magnetron sputtered WS2/a-C coatings. Surf Coat Technol 2017;332:142–52. https://doi.org/10.1016/j.surfcoat.2017.06.087.

[66] Caessa J, Vuchkov T, Yaqub TBin, Cavaleiro A. On the microstructural, mechanical and tribological properties of Mo-Se-C coatings and their potential for friction reduction against rubber. Materials 2021;14. https://doi.org/10.3390/ma14061336.

[67] Voevodin AA, Zabinski JS. Supertough wear-resistant coatings with "chameleon" surface adaptation. Thin Solid Films 2000;370:223–31. https://doi.org/10.1016/S0040-6090(00)00917-2.

[68] Voevodin AA, Zabinski JS. Load-adaptive crystalline – amorphous nanocomposites. J Mater Sci 1998;33:319–27. https://doi.org/10.1023/A:1004307426887.

[69] Dominguez-Meister S, Justo A, Sanchez-Lopez JC. Synthesis and tribological properties of WSex films prepared by magnetron sputtering. Mater Chem Phys 2013;142:186–94. https://doi.org/10.1016/j.matchemphys.2013.07.004.

[70] Grigoriev SN, Fominski VY, Gnedovets AG, Romanov RI. Experimental and numerical study of the chemical composition of WSex thin films obtained by pulsed laser deposition in vacuum and in a buffer gas atmosphere. Appl Surf Sci 2012;258:7000–7. https://doi.org/10.1016/j.apsusc.2012.03.153.

[71] Rasamani KD, Alimohammadi F, Sun Y. Interlayer-expanded MoS 2. Mater Today 2017;20. https://doi.org/10.1016/j.mattod.2016.10.004.

[72] Vuchkov T, Evaristo M, Yaqub TBin, Polcar T, Cavaleiro A. Synthesis, microstructure and mechanical properties of W–S–C self-lubricant thin films deposited by magnetron sputtering. Tribol Int 2020;150. https://doi.org/10.1016/j.triboint.2020.106363.

[73] Yaqub TBin, Vuchkov T, Bruyère S, Pierson JF, Cavaleiro A. A revised interpretation of the mechanisms governing low friction tribolayer formation in alloyed-TMD self-lubricating coatings. Appl Surf Sci 2022;571. https://doi.org/10.1016/j.apsusc.2021.151302.

[74] Muratore C, Voevodin AA. Control of molybdenum disulfide basal plane orientation during coating growth in pulsed magnetron sputtering discharges. Thin Solid Films 2009;517:5605–10. https://doi.org/10.1016/j.tsf.2009.01.190.

[75] Mikhailov S, Savan A, Pflüger E, Knoblauch L, Hauert R, Simmonds M, et al. Morphology and tribological properties of metal (oxide)–MoS2 nanostructured multilayer coatings. Surf Coat Technol 1998;105:175–83. https://doi.org/10.1016/S0257-8972(98)00483-6.

[76] Simmonds MC, Savan A, Swygenhoven HVan, Pflüger E, Mikhailov S. Structural, morphological, chemical and tribological investigations of sputter deposited MoSx/metal multilayer coatings. Surf Coat Technol 1998;108–109:340–4. https://doi.org/10.1016/S0257-8972(98)00567-2.

[77] Zhu J, Zeng Q, Zhang B, Yan C, He W. Elevated-temperature super-lubrication performance analysis of dispersion-strengthened WSN coatings: experimental research and first-principles calculation. Surf Coat Technol 2021;406. https://doi.org/10.1016/j.surfcoat.2020.126651.